CHARACTERISTICS OF IONOSPHERIC DISTURBANCES ACCOMPANYING THE MAGNETIC STORM OF JANUARY 14-20, 2022 г.

©2025 V. I. Kurkin [1,*], N. A. Zolotukhina [1,**], S. N. Ponomarchuk [1,***], A. V. Oinats [1,****], K. G. Ratovsky [1,*****]

[1] *Institute of Solar-Terrestrial Physics SB RAS (ISTP SB RAS), Irkutsk, Russia*

[*] *e-mail: vikurkin @ yandex.ru*

[**] *e-mail: zolot@iszf.irk.ru*

[***] *e-mail: spon@iszf.irk.ru*

[****] *e-mail: oinats@iszf.irk.ru*

[*****] *e-mail: ratovsky@iszf.irk.ru*

Received February 14, 2024

Revised May 06, 2024

Accepted July 25, 2024

An analysis of ionospheric disturbances accompanying the moderate magnetic storm of January 14-20, 2022 has been conducted. The work is based on vertical and oblique ionospheric sounding data obtained in the North-Eastern region of Russia, supplemented by observations from HF radars and magnetic observatories. It was revealed that the amplitudes of positive and negative ionospheric disturbances accompanying this storm are comparable with disturbances observed on other days in January during weak magnetic storms and disturbances. Specific features of disturbances observed only during the studied storm include: (1) midnight-morning increase in the maximum observed frequency of one-hop propagation mode of HF radio waves on the Norilsk-Tory and Magadan-Tory paths on January 14; (2) nighttime enhancement of fluctuations in the critical frequency of the *F* 2-layer in Irkutsk and the maximum observed frequency of one-hop mode on the Magadan-Tory path on January 15; (3) morning-noon *Es layers* with limiting frequencies reaching 7 MHz, observed at middle latitudes at the end of the first and beginning of the second day of the recovery phase of the storm.

DOI: 10.31857/S00167940250109e9

1. INTRODUCTION

Studies of the influence of solar and geomagnetic activity on radio wave propagation conditions, which began in the late 1920s [Pickard, 1927; Anderson, 1928], established a close connection between geomagnetic disturbances and significant changes in the ionospheric structure. Based on the results of these studies, the term "ionospheric storm" was introduced, which refers to the set of ionospheric disturbances accompanying geomagnetic storms. Currently, the study of ionospheric storms is developing very intensively in both observational and theoretical directions. Interest in this phenomenon is due to the fact that ionospheric disturbances often disrupt the operation of ionospheric radio communication systems, causing interference, and in extreme cases the absence of radio wave propagation between receiving and transmitting devices, as well as energy systems, leading to partial or complete power outages, failures in railway automation, etc. [Goodman et al., 2006; Kuznetsov, 2014; Pilipenko, 2021].

To study the spatial-temporal dynamics of an ionospheric storm, it is customary to use the difference between current and background values of the critical frequency of the $F2$ layer of the ionosphere ($foF2$) or the maximum electron concentration of the ionosphere determined from it $NmF2 = 1.24\times10^{4}(foF2)^{2}$, as well as between current and background values of total electron content (TEC). Based on the sign of this difference, ionospheric disturbances are divided into positive and negative ones, which are considered the main elements of an ionospheric storm. As background values, the average values of $foF2$/TEC measured on the magnetically quiet days (q-days) closest to the beginning of the storm, or their monthly median values are usually used [Danilov, 2013; Mikhailov et al., 2004]. However, significant changes in ionospheric parameters, comparable with changes occurring during storms, are observed even on q-days, which requires verification of the validity of using these days to determine the background in each specific case [Perrone et al., 2020]. The second method is more acceptable when the values of $foF2$/TEC measured on magnetically quiet days significantly differ from their monthly median values. In addition to positive and negative disturbances of various amplitudes and durations, an ionospheric storm includes enhanced formation of sporadic and diffuse ionospheric layers.

The spatial-temporal scales and intensity of ionospheric disturbances, as well as the level of geomagnetic activity, increase with the growth of corpuscular and electromagnetic energy entering from the interplanetary medium initially into the high-latitude part of the magnetosphere-ionosphere system, and then into other regions of the outer geospheres [Prölss, 2006]. The strongest magnetosphere-ionosphere disturbances occur during the years of solar activity maximum.

The generalized spatial-temporal pattern of ionospheric storm development is based mainly on data obtained during isolated strong and moderate magnetic storms with clearly expressed main, recovery, and in some cases, initial phase [Prölss, 1997; Fuller-Rowell et al., 1997; Buonsanto, 1999; Mendillo, 2006; Danilov, 2013]. It has been established that the manifestations of an ionospheric storm registered by a specific ionosonde depend not only on interplanetary, magnetospheric and thermospheric processes, but also on the location of the observation point and its local time [Zherebtsov and Pirog, 2008; Kurkin et al., 2008].

Much less information has been collected to date about ionospheric disturbances accompanying weak magnetic storms, which at middle latitudes can be comparable with changes during strong magnetic storms [Buresova et al., 2014]. Decrease in the maximum observed frequencies of one-hop mode of HF radio wave propagation *F* 2 (MUF1 F2) during weak magnetic storms can be 25–50% [Kurkin et al., 2022; Kurkin et al., 2022]. The paper [Ratovsky et al., 2022] shows that about half of the 25 extreme increases in the maximum electron density in the ionospheric *F* 2-layer observed in Irkutsk in 2003–2016, where normalized deviations of *NmF* 2 from monthly median values were more than 150%, were observed during weak geomagnetic disturbances with a minimum $Dst > -30$ nT. According to the criterion specified in the paper [Gonzalez et al., 1994], disturbances with a *Dst* index > -30 nT are not geomagnetic storms.

An attempt at a statistical study of the ionospheric response to "weaker" geomagnetic activity was undertaken in the publication [Chen et al., 2022]. To select "weaker" events, the authors used the criterion $Ap < 60$. As a result of applying this criterion, the sample analyzed in the work [Chen et al., 2022] included strong and moderate magnetic storms, which calls into question the validity of the conclusions made in this work regarding trends in the ionospheric response to weak magnetic disturbances. Another significant drawback of the work [Chen et al., 2022], which calls its conclusions into question, is the heterogeneity of the experimental data on which it is based.

This paper continues the study of the ionospheric response to weak magnetic storms, initiated in the work [Kurkin et al., 2022; Kurkin et al., 2022], which shows that the ionospheric response to the impact of a high-speed solar wind stream causing a storm depends both on the geoeffective parameters of the stream, and on the duration of its impact on the magnetosphere-ionosphere system and its initial state.

2. OBJECT AND PURPOSE OF THE STUDY

Ionospheric data obtained in January 2022 during the growth phase of the 25th solar activity cycle were selected for the study. The analysis of the geomagnetic environment is based on series of

values of *Kp* , *Dst, ap* [URL OMNI2], and *SME* [URL SME] indices. Characteristics of interplanetary sources that caused geomagnetic disturbances are presented in the work through parameters of solar wind (SW) plasma and interplanetary magnetic field (IMF) [URL OMNI2]. Based on SW and IMF parameters, the Akasofu parameter ε (energy flux incident from the interplanetary medium onto the subsolar magnetosphere [Akasofu, 1981]) was calculated.

Fig. 1.

Fig. 1 shows that during the selected month, the magnetosphere-ionosphere system was affected by 4 high-speed solar wind streams with peak velocities greater than 450 km/s. The first stream caused weak disturbances on January 1-4 with a minimum *Dst* = -25 nT and maximum *Kp* = 4; the second, slower stream on January 8-11, caused a weak storm on January 8-11 with an increase in *Kp* to storm level *Kp* = 5 and a decrease in *Dst* to -27 nT.

The disturbances on January 14-20 constitute a moderate magnetic storm (minimum *Dst* = -91 nT, maximum *Kp* = 6-). It was caused by a complex interplanetary inhomogeneity formed by an interplanetary coronal mass ejection, a high-speed solar wind stream from coronal hole *CH* 1054 catching up to it, and two more coronal ejections. The wind speed increased non-monotonically from 360 km/s in the leading part of the inhomogeneity to 700 km/s on the penultimate day of the storm. At the leading edge of the inhomogeneity, the southward vertical component of the interplanetary magnetic field (*Bz* IMF) intensified to -17 nT (not shown in the figure). Panel (*b*) shows that the power of the external source of the January 14-20 storm, estimated using the Akasofu parameter (ε), was approximately 2 times greater than the power of interplanetary sources of other disturbances. One should expect that this storm was accompanied by stronger ionospheric disturbances than those observed during other events.

Series of weak disturbances on January 22-23 and 25-31 were characterized by multiple decreases in *Dst* , of which only 2 can be classified according to the minimum *Dst* = -34 and -44 nT (January 25 and 31, respectively) as weak magnetic storms.

It should be noted that in January 2022, there was no sudden stratospheric warming, which, according to Mikhailov et al. [2021], has a significant impact on the development of ionospheric disturbances [Vargin et al., 2022]. However, at ~04:15 UT on January 15, a powerful eruption of the Tonga volcano occurred, causing the generation of traveling ionospheric disturbances (TIDs) with main periods of ~10-30 min, propagating along the great circle at a speed of 300-350 m/s [Zhang et al., 2022].

The specific goal of our work is to compare ionospheric disturbances that developed during the moderate storm of January 14-20 with those disturbances that were observed on other days of January 2022, including days of weak storms and *q* -days.

3. ANALYZED DATA

The study is based on series of monthly values of critical frequency and peak height of the *F* 2-layer (*foF* 2 and *hmF* 2), the limiting frequency of the *Es-layer* (*foEs*) as well as measurements of MUF1 *F* 2, obtained on oblique sounding (OS) paths of the ionosphere.

Values *foF* 2 , *hmF* 2, *foEs* were measured using an ionosonde *DPS* -4 and a chirp ionosonde located in Irkutsk (52.5° N, 104° E, Φ = 48.4°) with Δ *t* =15 min and in Tory, Republic of Buryatia (52° N, 103° E, Φ = 48°) with duty cycle Δ *t* =1 min. Here Φ — corrected geomagnetic latitude. Additionally, observations of auroral echo in Yekaterinburg (*EKB*) and Magadan (*MGW*) on HF radars, series of values of the horizontal (*H*) component of the geomagnetic field measured at the observatories of Irkutsk, Yakutsk (62° N, 129.7° E, Φ = 56.8°) [URL Intermag] and original data from the magnetic observatory of Norilsk (69.4° N, 88.1° E, Φ = 65.3°), as well as the coordinates of the polar and equatorial boundaries of the auroral oval taken from the website [URL Oval]. The map of observation facilities is shown in Fig. 2.

Fig. 2.

Measurements of MUF1 *F* 2 were carried out with a duty cycle Δ *t* =5 min on the Norilsk-Tory and Magadan-Tory paths (coordinates of the midpoints of the paths 60.9° N, 98° E , Φ = 57° and 58.5° N, 125.8° E, Φ = 53.7° respectively).

Continuous monitoring on these paths was carried out using the equipment of the multifunctional chirp ionosonde "Ionosonde-MS" [Podlesny et al., 2013]. The northern section of the first path is located in subauroral latitudes. The Magadan-Tory path belongs to mid-latitudes, but during strong magnetic disturbances, its northern section, including the midpoint, can be located in the main ionospheric trough (MIT) [Polekh et al., 2016]. In our work, the corrected geomagnetic latitude (Φ) of the MIT bottom is determined using the model presented in the paper [Deminov and Shubin, 2018]. In it, the latitude of the MIT bottom is calculated based on the values of *ap* -index in the current and several (in our case, 4) preceding 3-hour intervals.

4. IONOSPHERIC STORM JANUARY 14-20, 2022

Fig. 3.

On the three lower panels of Fig. 3, there are graphs showing changes in MUF1 *F* 2 for two paths and *foF* 2, *foEs* over Irkutsk, constructed from original data obtained during the 4 days preceding the moderate storm of January 14-20, and during the storm. For convenience of comparison, the upper panel shows a graph of the *Dst-index change.* index.

The magnetic storm began around 16 UT on January 14 with the main phase and continued until the end of January 20. During the magnetically quiet days of January 10-13 preceding the storm, nighttime positive ionospheric disturbances were recorded on the Magadan-Tory path and in Irkutsk. At this time, the values of MUF1 *F* 2 were about ~2 MHz, and *foF* 2 were about ~1.5 MHz higher than the monthly median values (shown in the figure with a gray line). The authors of the paper [Mikhailov et al . , 2004] call such events "Q disturbances" and believe that they are genetically related to planetary waves. Due to the presence of nighttime Q disturbances, we selected monthly median values of ionospheric parameters as background values.

The graphs presented in Fig. 3 show that in our longitude sector, the ionospheric storm began before 19:00 UT on January 14, approximately 3 hours after the beginning of the main phase of the magnetic storm, and ended after 5 days (around 14:00 UT on January 19, the penultimate day of the late recovery phase of the storm). Let us point out the disturbances clearly visible in the graphs, which may be manifestations of the ionospheric storm.

4.1. Positive ionospheric disturbance observed on the Norilsk-Tory path at 18:53-23:53 UT on January 14 after a 200-minute blackout, and a sharp increase in MUF1 *F* 2 from 8 to 13.6 MHz, recorded on the Magadan-Tory path at 22:00-22:05 UT on January 14 (between two sounding sessions) after a negative disturbance. In F ig. 3, these elements are marked with black arrows. On the Norilsk-Tory path, the disturbance was at its maximum at 20:58-21:13 UT on January 14.

4.2. Daytime negative disturbance highlighted by ovals, recorded on the Magadan–Tory path at 23:45–04:50 UT on January 14–15 and partially overlapping in time with a prolonged daytime positive disturbance that developed over Irkutsk at 02:00–09:00 UT on January 15.

4.3. Enhancement of short-period variations in MUF1 *F* 2 and *foF* 2 during nighttime hours on January 15 on the Magadan–Tory path (at 10–21 UT; 18.5–05.5 LT) and over Irkutsk (at 13–22 UT; 20–05 LT). In Fig. 3, these intervals are marked by gray rectangles on the abscissa axis of panels *c* , *d.* The average period of variations $T \approx 110–120$ min.

4.4. The intensification of diffuse morning (gray arrow on panel *d*) and daytime (black rectangle on the abscissa axis of panel *d*) flat sporadic layers with high critical frequencies observed in Irkutsk and Tory, with maximum values equal to 7 and 5.5 MHz respectively.

4.5. Nighttime negative disturbances marked by ovals, observed in Irkutsk and on the Magadan–Tory path on January 16 in similar time intervals. On the Magadan–Tory path, the nighttime negative disturbance transitioned into a weaker daytime negative disturbance that continued until 05:00 UT on January 17.

4.6. The last notable ionospheric disturbance (highlighted by a gray rectangle) was observed simultaneously on the Magadan–Tory path and in Irkutsk at 09:30–13:00 UT (evening hours) on January 19. At the maximum of the disturbance, the current values of MUF1 *F* 2 and *foF* 2 were 60 and 40% higher than the background values, respectively.

5. DISCUSSION

To compare the elements of the ionospheric storm of January 14–20, 2022, described in Section 4, with ionospheric disturbances observed on other days of this month, we extracted short-period (periods $0.5 < T \leq 3.5$ h, the range of large-scale and medium-scale TIDs [Hunsucker, 1982]) and prolonged ($36 > T > 3.5$ h) disturbances from the original data series. For this procedure, a bandpass filter was used, which does not create phase shifts [Marmet, 1979]. Changes in the normalized deviations of prolonged disturbances of MUF1 *F* 2 and *foF* 2 (ΔMUF1 *F* 2 and Δ*foF* 2), observed during the month, from their background values (determined for the same periods) are shown in Fig. 4.

Fig. 4.

Let us indicate those specific elements of the ionospheric storm of January 14-20, 2022, which significantly differ from disturbances that occurred on other days.

5.1. First of all, this is the ionospheric disturbance mentioned in section *4.1.* the only explicit ionospheric disturbance observed in January 2022 on the Norilsk-Tory path. It developed as an increase in MUF1 *F* 2, which began during the main phase of the storm around 19 UT on January 14 and reached a maximum value of Δ*foF* 2 ~ 140%, which is 3-6 times greater than the positive disturbances observed on other days. The left panels of Fig. 5 show that the growth of MUF1 *F* 2 began after the trough minimum shifted to a latitude less than Φ of the midpoint of the path. The abrupt increase in *4.1.* in MUF1 MUF1 *F* 2 on the Magadan-Tory path at 22:00-22:05 UT also occurred after the midpoint of the path transitioned from the equatorial to the polar wall of the main ionospheric trough. Analysis of oblique sounding ionograms showed that the increase in MUF1 *F* 2 during this time period is due to multipath propagation of the 1 *F* 2 mode, as the polar wall of the trough approaches closely to the middle reflecting region of the ionosphere of the radio path Magadan - Tory. In addition, auroral precipitations during the *F* 2, manifestations of which

in geomagnetic variations are shown in Fig. 5 on the right. substorm could have made an additional contribution to the increase in MUF1

Fig. 5.

At the subauroral st. Yakutsk, the rapid decrease *of the H* -component of the magnetic field, characteristic of the explosive phase of a substorm, coincided in time with an increase *in the SME* -index by ~ 400 nT [URL *SME*]. It began approximately 5 minutes after the sharp increase in MUF1 *F* 2 on the Magadan-Tory path. At the auroral obs. Norilsk and mid-latitude obs. Irkutsk, negative and positive disturbances of *H* respectively began ~ 40 minutes later, indicating the progression of substorm phenomena toward the west. According to MGW-radar data, the development of the substorm was accompanied by an increase in Doppler velocities of auroral echo to the maximum values for this storm of ± 400 m/s. The echo signals came from a sector including the Yakutsk meridian, and their sources were located in the vicinity of the equatorial boundary of the auroral oval (see Fig. 6). At the same time, north of this boundary, the velocities were directed westward; south of it — eastward, toward the radar, which corresponds to the region of enhanced western electrojet.

Fig. 6.

Fig. 7.

5.2 . The second specific element of the considered ionospheric storm is the intensification of short-period variations of MUF1 *F* 2 and *foF* 2 during the night hours of January 15, noted in paragraph *4.3* . Figure 7 shows that on the Magadan-Tory path, the intensification of short-period variations of MUF1 *F* 2 (marked by an arrow with a broken line) was observed at 10-21 UT (18.5-05.5 LT) on January 15. In this interval, the standard deviation of MUF1 *F* 2 was 0.8 MHz, while during the same hours on other days it was 2 times less, only 0.4 MHz. Over Irkutsk, the intensification of short-period variations of *foF* 2 (marked by an arrow) occurred approximately one hour later — at 13-22 UT (20-05 LT). It was characterized by the standard deviation $S = 0.24$ MHz, approximately 2.5 times greater than on other days ($S = 0.1$ MHz). A less significant (approximately 1.5 times, up to $S = 0.6$ MHz) increase in short-period variations of MUF1 *F* 2 was also observed during 10-21 UT on January 9 only on the Magadan-Tory path. This interval is also marked with a broken line arrow. Comparing the graphs, we see that in both cases, nighttime activations of short-period components of MUF1 *F* 2 variations occurred during the recovery phase of moderate and weak magnetic storms, approximately one day after the MDP bottom shifted to the midpoint of the path.

The amplitudes of short-period variations of MUF1 *F* 2 and *foF* 2 observed during daytime hours in January 2022 (not shown in the figure) were 3 times larger ($S = 1.02$ and 0.32 MHz respectively) than the amplitudes of nighttime variations. They changed slightly from day to day, including during the transition from magnetically quiet days of January 10-13 to the magnetically disturbed day of January 15. The average period of the observed variations $T \approx$ 110-120 min. It is close to the period of TIDs T =1.8 h, associated with geomagnetic storms [Ding et al., 2008]. However, the permanent nature of the short-period variations of MUF1 *F* 2 and *foF* 2 presented in the article does not allow their identification with TIDs, which episodically occur at high latitudes during geomagnetic disturbances [Hunsucker, 1982].

Fig. 8.

5.3. We also classified as special elements of the ionospheric storm the activation of flat mid-latitude sporadic layers mentioned in item 4.4 . during morning and daytime hours of January 15-16. The upper left panel of Fig. 8 shows that sporadic layers with *foEs* from 1 to 7 MHz were observed daily. The number of sessions in which their critical frequencies were greater than 3.1 MHz (upper quartile of the monthly series of *foEs* values), varied from day to day from 1 to 17. The maximum number of ionograms with *foEs* > 3.1 MHz was obtained in 17 of 18 sessions conducted at 03:30-07:45 UT (10:30-14:30 LT) on January 16. The lower left panel of Fig. 8 shows that during these hours, the activation of sporadic layers was observed only on January 16. The features of this ionospheric storm also include the activation of morning sporadic layers at 20:45-22:45 UT (03:45-05:45 LT) on January 15, during which the highest critical frequencies for January 2022 of 5.6, 6.9, and 6.6 MHz were recorded in three consecutive sessions. In the morning hours, the value of *foEs* = 6.6 MHz, close to that observed on January 15, was recorded only on January 2 in 1 of 96 sessions conducted that day. In [Tang et al., 2022], it is shown that the formation of dense *Es* -layers at mid-latitudes during geomagnetic storms may be related to wind enhancement in the mesosphere and lower thermosphere.

5.4. The specifics of the positive and negative ionospheric disturbances noted in sections 4.2, 4.5, and 4.6 , can be judged from the graphs shown in Figures 4, 5, 9, and 10.

Fig. 9.

Fig. 9 presents separately the positive (panel *a*) and negative (panel *b*) values of ΔMUF1 *F* 2 on the Magadan-Tory path for each day of January 2022. Below them is shown the time of registration of positive values of ΔMUF1 *F* 2 lying above the upper quartile, and negative values lying below the lower quartile , of the monthly series of these parameters. In the same format, panels (*c*) and (*d*) of Fig. 9 present positive and negative values of Δ *foF* 2 obtained in Irkutsk.

5.4.1. It can be seen that the relatively weak daytime positive disturbance with $\Delta foF2 \leq 23\%$, registered in Irkutsk at 02-09 UT (09-16 LT) on January 15 (see section *4.2*) was earlier than the evening positive disturbance of greater magnitude with $\Delta foF2 \sim 40$ % on January 19 (see section *4.6.*) and less significant evening positive disturbances with $\Delta foF2 \sim 25$–38%, observed in Irkutsk at 08–13 UT (15–20 LT) on January 25 and 27–31.

The second feature of the positive disturbance of *foF* 2 on January 15 is that it corresponds to a decrease in MUF1 *F* 2 on the Magadan–Tory path. In contrast, evening positive disturbances of *foF* 2 on January 19, 25, and 27 are observed almost simultaneously with evening positive disturbances of MUF1 *F* 2 on the Magadan–Tory path. This was especially pronounced in the evening hours of January 19 during the intensification of the ring current field and on January 25 during a weak magnetic storm (see Fig. 1 and Fig. 4). Judging by morphological characteristics, the evening positive disturbances are manifestations of the Dusk Effect [Buonsanto, 1999]. Returning to Fig. 5, we can see that the decrease in MUF1 *F* 2 on the Magadan–Tory path in the first hours of January 15 followed the crossing of the TID trough by the midpoint of the path.

Fig. 10.

The third difference between the daytime positive disturbance on January 15 and the dusk effects is shown in the upper panels of Fig. 10. It can be seen that *foF* 2 values increase during the rise of the peak height of the *F* 2-layer (panel *a*), while in cases of dusk effects (panels *b* , *c*) there is a decrease in *hmF* 2.

Note that daytime positive disturbances of *NmF* 2 are characteristic of middle latitudes in winter months [Buonsanto, 1999]. In the paper [Paznukhov et al., 2009] it is shown that at middle latitudes, positive ionospheric disturbances observed during geomagnetic storms lag behind the increase in peak height of the *F* 2-layer. The delay between the increase in *hmF* 2 and *foF* 2 is 1-2 hours. In our case, it is about $\Delta t \approx 1.5$ h. The onset time of the positive phase of the ionospheric storm depends on the local time of the observation point at the beginning of the geomagnetic storm. Using the graph shown in Fig. 10 in [Paznukhov et al., 2009], we found that the positive ionospheric disturbance could have started in Irkutsk 8-9 hours after the beginning of the storm, that is at 00-01 UT, which corresponds, as well as the value of Δt , to the results of our analysis of experimental data.

Collectively, these differences indicate that during the daytime hours of 15.01.2022 in the considered longitudinal sector at middle latitudes, the influence of the equatorward wind prevailed, while at subauroral latitudes, the movement of LSTIDs and, possibly, changes in atmospheric composition were dominant.

5.4.2. In section *4.5* . of the previous section, we noted that on 16.01.2022, a nighttime negative ionospheric disturbance was observed almost simultaneously on the Magadan-Tory path and in Irkutsk. This is clearly seen in Fig. 3, as well as in Fig. 9 (panels *b* , *d*), where this disturbance is marked with arrows. In these panels it can be seen that negative disturbances comparable in depth and appearance time to the negative disturbance of January 16 were observed on the Magadan-Tory path during weak geomagnetic disturbances on January 1 and 2. In Irkutsk, the negative disturbances closest to it in depth ($\Delta foF2 \approx$ -40%) were observed on magnetically quiet days of January 6 and 7, and in terms of appearance time on 27.01 . 2022, during the recovery phase of a weak magnetic storm. However, on January 6 and 7, the decreases in *foF* 2 were observed not during nighttime, but during noon-evening hours, and the disturbance on January 27 had a much smaller depth $\Delta foF2 \approx$ -30%.

The graphs shown in Fig. 10 (panels *g – e*) demonstrate the trend of increasing *hmF* 2 during negative ionospheric disturbances that developed over the North-Eastern region of Russia in January 2022.

6. CONCLUSIONS

Analysis of vertical and oblique sounding data obtained in the North-Eastern region of Russia in January 2022 showed that the ionospheric storm accompanying the magnetic storm of January 14-20, 2022, contained the following elements not observed on other days of this month .

1. Prolonged increase in MUF1 *F* 2 on the Norilsk-Tory path, which began on January 14 3 hours after the start of the main phase with an increase in MUF1 *F* 2 relative to the background by 100% and, after 2 hours, by ΔMUF1 *F* 2 = 120%.

2. A sharp increase in MUF1 F *F* 2 by 5.6 MHz (by ~70%) that occurred between 2 sounding sessions on the Magadan-Tory path. It was registered on January 14, 6 hours after the start of the main phase.

3. Intensification of disturbances in *foF* 2 and MUF1 *F* 2 with periods of 0.5-3.5 hours, observed over Irkutsk and on the Magadan-Tory path during the night hours of January 15 (the first day of the recovery phase of the storm).

4. Sporadic layers with high critical frequencies, continuously recorded in Irkutsk for 4 daytime hours on January 16 (the second day of the recovery phase of the storm).

Events 1 and 2 could be related to the position of the midpoints of radio paths relative to the polar and equatorial "walls" of the Main Ionospheric Trough (MIT). At the polar wall of the MIT, i.e., in the zone of diffuse precipitation, the electron concentration increases during geomagnetic disturbances. The sharp increase in MUF1 *F* 2 on the Magadan-Tory path could be associated with

a substorm that made an additional contribution to the flux of precipitating electrons. The substorm was registered at the subauroral observatory Yakutsk, located near the midpoint of the Magadan-Tory path.

Causes of intensification of MUF1 *F* 2 fluctuations and *foF* 2 on January 15 and the formation of mid-latitude sporadic layers on January 15-16 are not entirely clear. Based on satellite data obtained near the libration point L1, we believe that the activation of nighttime disturbances with periods of 0.5-3.5 hours during the recovery phase of the storm could be associated with the intensification of thermospheric wind and the impact of fluctuations in solar wind pressure and interplanetary magnetic field on the metastable magnetosphere-ionosphere system.

The prolonged positive disturbance observed in Irkutsk during daytime hours on January 15 developed against the background of an increase in the height of the *F* 2-layer maximum and negative ionospheric disturbance on the Magadan-Tory path. Together this indicates that during the daytime hours of 01.15.2022 in the considered longitudinal sector at middle latitudes, the influence of equatorward wind prevailed, and in subauroral latitudes — the shift of the TID bottom to the latitude of the midpoint of the Magadan-Tory path and changes in atmospheric composition.

ACKNOWLEDGMENTS

The results were obtained based on observations conducted using the equipment of the "Angara" Shared Use Center (http://ckp-angara.iszf.irk.ru/). We thank the managers of websites (https://wdc.kugi.kyoto-u.ac.jp/qddays/index.html), (https://intermagnet.org), (https://cdaweb.gsfc.nasa.gov/cdaweb/istp_public), (https://ssusi.jhuapl.edu/gal_edr-aur_cs) and the SuperMAG collaboration (https://supermag.jhuapl.edu/indices/) for the opportunity to use information posted on their websites.

FUNDING

The research was carried out with financial support from the Ministry of Education and Science (subsidy No. 075-GZ/C3569/278).

REFERENCES

1. *Danilov A.D.* Response of the F region to geomagnetic disturbances (review) // Heliogeophysical Research. Issue 5. P. 1-33. 2013. http://vestnik.geospace.ru/index.php?id=189

2. *Deminov M.G., Shubin V.N.* Empirical model of the main ionospheric trough position // Geomagnetism and Aeronomy. V. 58. № 3. P. 366-373. 2018. https://doi.org/10.7868/S0016794018030070

3. *Zherebtsov G.A.*, *Pirog O.M.* Dynamics and macrostructure of ionospheric plasma / Encyclopedia of Low-Temperature Plasma. Series B. Reference applications, databases and data banks. Volume I–3. Ionospheric plasma. Part 1. Ed. V.D. Kuznetsov, Yu.Ya. Ruzhin. M: Yanus-K. P. 363-380. 2008.

4. *Kuznetsov V.D.* Space weather and space activity risks // Space Engineering and Technology. № 3 (6). P. 3-13. 2014. https://sciup.org/kosmicheskaja-pogoda-i-riski-kosmicheskoj-dejatelnosti-14343447

5. Kurkin V.I. , Polekh N.M., Zolotukhina N.A. Ionospheric effects of weak geomagnetic storms at the solar activity minimum: spring equinox / Proceedings of the All-Russian Open Scientific Conference Armand Readings: Modern Problems of Remote Sensing, Radar, Wave Propagation and Diffraction [Electronic resource]. P. 105-114. 2022. https://doi.org/10.24412/2304-0297-2022-1-105-114

6. *Pilipenko V.A.* Impact of space weather on ground-based technological systems // Solar-Terrestrial Physics. V. 7. № 3. P. 72-109. 2021. https://doi.org/ 10.12737/szf-73202106

7. *Podlesnyy A.V., Brynko I.G., Kurkin V.I., Berezovsky V.A., Kiselev A.M., Petukhov E.V.* Multifunctional LFM-ionosonde for ionosphere monitoring // Heliogeophysical Research. Iss. 4. P. 24-31. 2013. **http://vestnik.geospace.ru/index.php?id=166**

8. *Polekh N.M., Zolotukhina N.A., Romanova E.B., Ponomarchuk S.N., Kurkin V.I., Podlesnyy A.V* . Ionospheric effects of magnetospheric and thermospheric disturbances on March 17-19, 2015 // Geomagnetism and Aeronomy. V. 56. № 5. P. 591-605. 2016.

9. Akasofu S.I. Energy coupling between the solar wind and the magnetosphere // Space Sci. Rev. V. 28. N 2. P. 121-190. 1981. https://doi.org/10.1007/BF00218810

10. *Anderson C.N.* Correlation of long wave transatlantic radio transmission with other factors affected by solar activity // Proc. Inst. Radio Eng. V. 16. N 2. P. 297 - 347. 1928. https://doi.org/ 10.1109/JRPROC.1928.221400

11. Borovsky J.E., Denton M.H. Solar wind turbulence and shear: A superposed-epoch analysis of corotating interaction regions at 1 AU // J. Geophys. Res. V. 115. N A10101. 2010. https://doi.org/10.1029/2009JA014966

12. *Buonsanto M.J.* Ionospheric storms — a review // Space Sci. Rev. V. 88. N 3-4. P. 563-601. 1999. https://doi.org/10.1023/A:1005107532631

13. *Buresova D. Lastovicka J. Hejda P. Bochnicek J.* Ionospheric disturbances under low solar activity conditions // Adv. Space Res. V. 54. P. 185-196. 2014. https://doi.org/10.1016/j.asr.2014.04.007

14. *Chen Y., Liu L., Le H., Zhang H., Zhang R.* Responding trends of ionospheric F_2-layer to weaker geomagnetic activities // J. Space Weather Space Clim. V. 12. N 6. 12 pp. 2022. https://doi.org/10.1051/swsc/2022005

15. *Ding F., Wan W., Liu L., Afraimovich E.L., Voeykov S.V., Perevalova N.P.*A statistical study of large-scale traveling ionospheric disturbances observed by GPS TEC during major magnetic storms over the years 2003–2005 // J. Geophys. Res. V.113. N A00A01. 2008. https://doi.org/10.1029/2008JA013037

16. *Fuller-Rowell T.J., Codrescu M.V., Roble R.G., Richmond A.D.* How does the thermosphere and ionosphere react to a geomagnetic storm? / Magnetic Storms / AGU Geophysical Monograph Series. V. 98. Eds. B. T. Tsurutani, W. D. Gonzalez, Y. Kamide, J. K. Arballo. American Geophysical Union, Washington, D.C. P. 203 − 225. 1997.

17. *Gonzalez W.D ., Joselyn J.A., Kamide Y., Kroehl H.W., Rostoker G., Tsurutani B.T., Vasyliunas V.M.* What is a geomagnetic storm? // J. Geophys. Res. V. 99. Iss. A4. P. 5771–5792. 1994. https://doi.org/10.1029/93JA02867

18. *Goodman J.M., Ballard J.W., Patterson J.D., Gaffney B.* Practical measures for combating communication system impairments caused by large magnetic storms // Radio Sci. V. 41. N 6. RS6S41. 2006. https://doi.org/10.1029/2005RS003404

19. Hunsucker R.D. Atmospheric gravity waves generated in the high-latitude ionosphere: a review // J. Geophys. Res. V. 20. N 2. P. 293 − 315. 1982.

20. Kurkin V.I., Pirog O.M., Polekh N.M., Mikhalev A.V., Poddelsky I.N., Stepanov A.E. Ionospheric response to geomagnetic disturbances in the north-eastern region of Asia during the minimum of 23rd cycle of solar activity // J. Atmos. Sol.-Terr. Phys. V. 70. N 18. P. 2346–2357. 2008.

21. Kurkin V.I., Polekh N.M., Zolotukhina N.A. Effect of weak magnetic storms on the propagation of hf radio waves // Geomagnetism and Aeronomy. V. 62. № 1–2. P. 104–115. 2022. https://doi.org/ 10.1134/S0016793222020116

22. Loewe C.A., Prolss G.W. Classification and mean behavior of magnetic storm // J. Geophys. Res. V. 102. N A7. P. 14209–14213. 1997. https://doi.org/ 10.1029/96JA04020

23. Marmet P. New digital filter for the analysis of experimental data // Rev. Sci. Instrum. V. 50. N 1. P. 79–83. 1979. https://doi.org/ 10.1063/1.1135673

24. *Mendillo M.* Storms in the ionosphere: Patterns and processes for total electron content // Rev. Geophys. V. 44. RG4001. 2006. https://doi.org/10.1029/2005RG000193

25. *Mikhailov A.V., Depueva A.Kh., Leschinskaya T.Yu.* Morphology of quiet time *F* 2-layer disturbances: high and lower latitudes // Int. J. Geomagn. Aeron. V. 5. N 1. GI1006. 2004. https://doi.org/ 10.1029/2003GI000058

26. *Mikhailov A.V., Perrone L., Nusinov A.A.* Mid-latitude daytime *F* 2-layer disturbance mechanism under extremely low solar and geomagnetic activity in 2008–2009 // Remote Sens. 13. 1514. 2021. https://doi.org/10.3390/rs13081514

27. *Paznukhov V.V., Altadill D., Reinisch B.W.* Experimental evidence for the role of the neutral wind in the development of ionospheric storms in midlatitudes // J. Geophys. Res. V. 114. N A12319. 2009. https://doi.org/10.1029/2009JA014479

28. *Perrone L., Mikhailov A.V., Nusinov A.A.* Daytime mid-latitude *F* 2-layer Q-disturbances: A formation mechanism // Sci Rep. V. 10. 9997. 2020. https://doi.org/10.1038/s41598-020-66134-2

29. *Pickard G.W.* The correlation of radio reception with solar activity and terrestrial magnetism // Proc. Inst. Radio Eng. V. 15. N 2. P. 83 – 97. 1927. https://doi.org/10.1109/JRPROC.1927.221165

30. *Prölss G.W.* Magnetic storm associated perturbations of the upper atmosphere / Magnetic Storms / AGU Geophysical Monograph Series. V. 98. Eds. B.T. Tsurutani, W.D. Gonzalez, Y.Kamide, J.K. Arballo. American Geophysical Union, Washington, D.C. P. 227 – 241. 1997.

31. *Prölss G.W*. Ionospheric F-region storms: Unsolved problems / Characterizing the Ionosphere. Meeting Proc. RTO-MP-IST-056. Fairbanks, United States, 12–16 June 2006. Neuilly-sur-Seine, France. V. 10. P. 10-1–10-20. 2006.

32. Ratovsky K.G., Klimenko M.V., Dmitriev A.V., Medvedeva I.V. Relation of extreme ionospheric events with geomagnetic and meteorological activity // Atmosphere. V. 13. N 1. P. 146. 2022. https://doi.org/ 10.3390/atmos13010146

33. *Tang Q., Sun H., Du Z., Zhao J., Liu Y., Zhao Z., Feng X.* Unusual enhancement of midlatitude sporadic-E layers in response to a minor geomagnetic storm // Atmosphere. V.13. N 5. P. 816. 2022. https://doi.org/10.3390/atmos 13050816

34. *Vargin P.N., Koval A.V., Guryanov V.V.* Arctic stratosphere dynamical processes in the winter 2021–2022 // Atmosphere. V.13. N 10. P.1550. 2022. https://doi.org/10.3390/atmos13101550

35. *Zhang S-R., Vierinen J., Aa E. et al.* Tonga volcanic eruption induced global propagation of ionospheric disturbances via Lamb Waves // Front. Astron. Space Sci. 9:871275. 2022. https://doi.org/ 10.3389/fspas.2022.871275
36. URL Intermag: https://intermagnet.org/
37. URL qd: https://wdc.kugi.kyoto-u.ac.jp/qddays/index.html
38. URL OMNI2 : https://cdaweb.gsfc.nasa.gov/cdaweb/istp_public/
39. URL Oval: https://ssusi.jhuapl.edu/gal_edr-aur_cs
40. URL SME: https://supermag.jhuapl.edu/indices/

Figure Captions

Fig. 1. Variations of the solar wind velocity *Vsw* (*a*); Akasofu parameter ε (*b*); *Dst* - (*c*) and *Kp* - (*d*) indices in January 2022. Horizontal lines mark on panel (*a*) — the value of *Vsw* = 450 km/s, used to identify high-speed streams [Borovsky and Denton, 2010]; on panel (*c*) — the levels *Dst* = –30 and –50 nT, which are the upper threshold values for weak and moderate magnetic storms respectively [Loewe and Prolss, 1997]; on panel (*d*) — the level *Kp* =5, used as the lower threshold for identifying magnetic storms. Symbols *q* and *d* with numbers mark magnetically quiet and disturbed days according to their designations on [URL qd].

Fig. 2. Map showing the location of ionospheric sounding instruments and magnetic observatories. Dots show ionospheric stations and magnetic observatories; dashed and solid lines − radio paths and radar beams respectively, crosses – midpoints of radio paths.

Fig. 3. Variations of the *Dst* index (*a*); MUF1 *F* 2 on Norilsk–Tory (*b*) and Magadan–Tory (*c*) paths; *foF* 2 and *foEs* in Irkutsk (*d*). Current/background values of MUF1 *F* 2 and *foF* 2 are shown by black/gray lines, values of *foEs* — by squares.

Fig. 4. The upper panel shows variations of the *Dst index;* index; below — ΔMUF1 *F* 2 on Norilsk–Tory, Magadan–Tory paths and Δ *foF* 2 over Irkutsk. Black arrows mark the elements of the ionospheric storm presented in sections 4.1, 4.2, 4.5, and 4.6 of Section 4 (see text).

Fig. 5. Left, from top to bottom: changes in the corrected geomagnetic latitude of the auroral oval (gray figure) and the MIA trough at longitudes 105 ° and 120 ° E (lines), MUF1 *F* 2 on the Norilsk–Tory and Magadan–Tory paths; right — graph of *SME index* and variations of the *H* -component of the geomagnetic field recorded by three observatories located in the considered longitudinal sector. The dynamics of the MIA trough is calculated using the model [Deminov and Shubin, 2018]. The boundaries of the oval are constructed using data provided at [URL Oval].

Fig. 6. Map of auroral echo sources recorded by two HF radars at 22:15 UT on 14.01.2022. Dashed/solid lines show the position of the northern/southern boundaries of the oval (constructed using data from [URL Oval]).

Fig. 7. Variations of the *Dst index,* MIA trough latitude and short-period components of MUF1 *F* 2 on the Magadan–Tory path and *foF* 2 in Irkutsk during nighttime.

Fig. 8. Top left shows *foEs* values measured in Irkutsk during each day of January 2022; bottom — recording time of *foEs* greater than 3.1 MHz. Here 3.1 MHz is the upper quartile of the monthly series of *foEs* values, marked on the figure by a horizontal dotted line. On the right is an ionogram containing reflections from the sporadic diffuse layer. It was obtained in Tory using a chirp ionosonde.

Fig. 9. (*a*) — Values of positive ΔMUF1 *F* 2 observed on the Magadan − Tory path during each day of January 2022 (top) and recording time of those that lie above the upper quartiles of monthly series of positive ΔMUF1 *F* 2 (bottom); (*b*) — the same for negative ΔMUF1 *F* 2 and those that lie below the lower quartiles of negative ΔMUF1 *F* 2. Panels (*c*) and (*d*) show similar graphs constructed for positive and negative Δ *foF* 2. Horizontal dashed lines mark the upper quartiles for positive and lower quartiles for negative disturbances.

Fig. 10. For positive (*a–c*) and negative (*d–f*) disturbances observed in Irkutsk in January 2022, changes in absolute deviations of *foF* 2 and *hmF* 2 from their background values are shown.

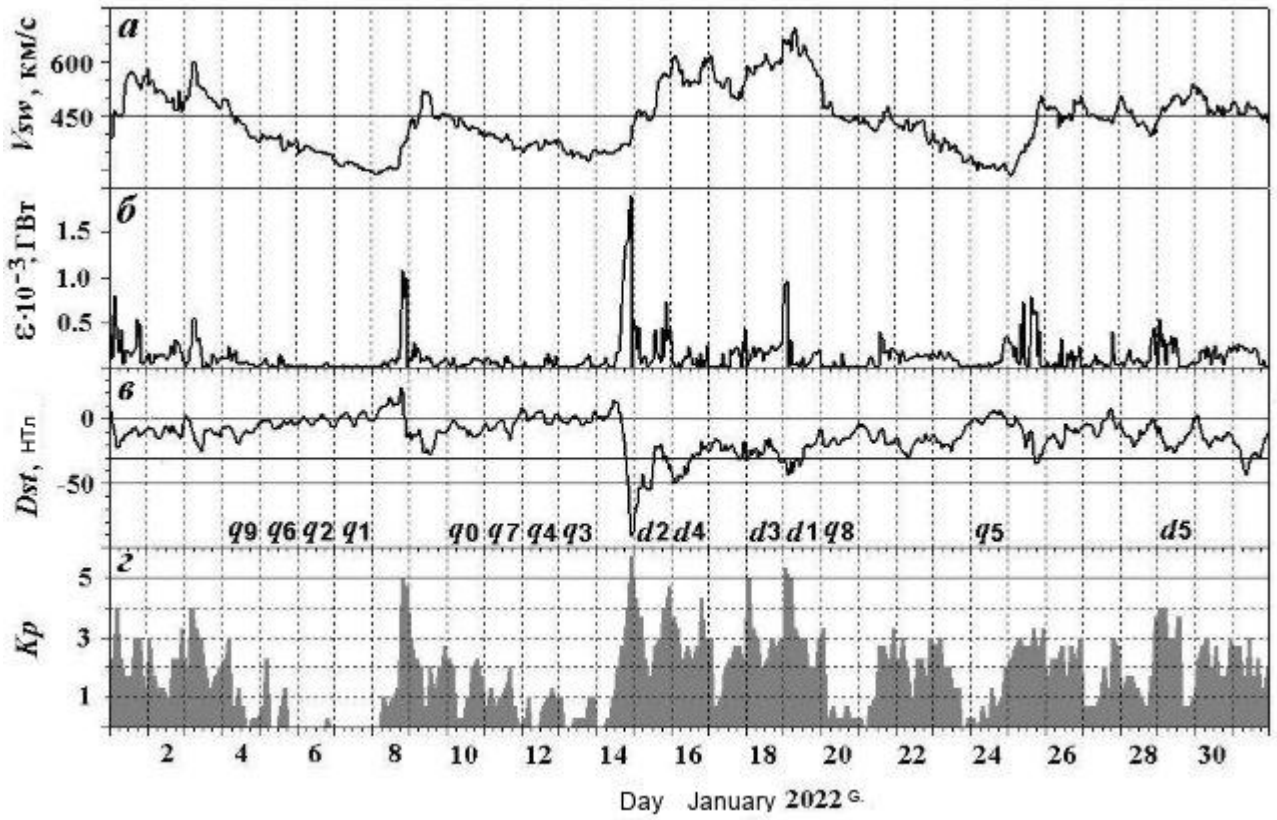
а
Vsw, км/с
600
450
б
ε·10⁻³, ГВт
1.5
1.0
0.5
в
Dst, нТл
0
-50
q9 q6 q2 q1
q0 q7 q4 q3
d2 d4
d3 d1 q8
q5
d5
г
Kp
5
3
1
2 4 6 8 10 12 14 16 18 20 22 24 26 28 30
Day January 2022 G.

Fig. 1

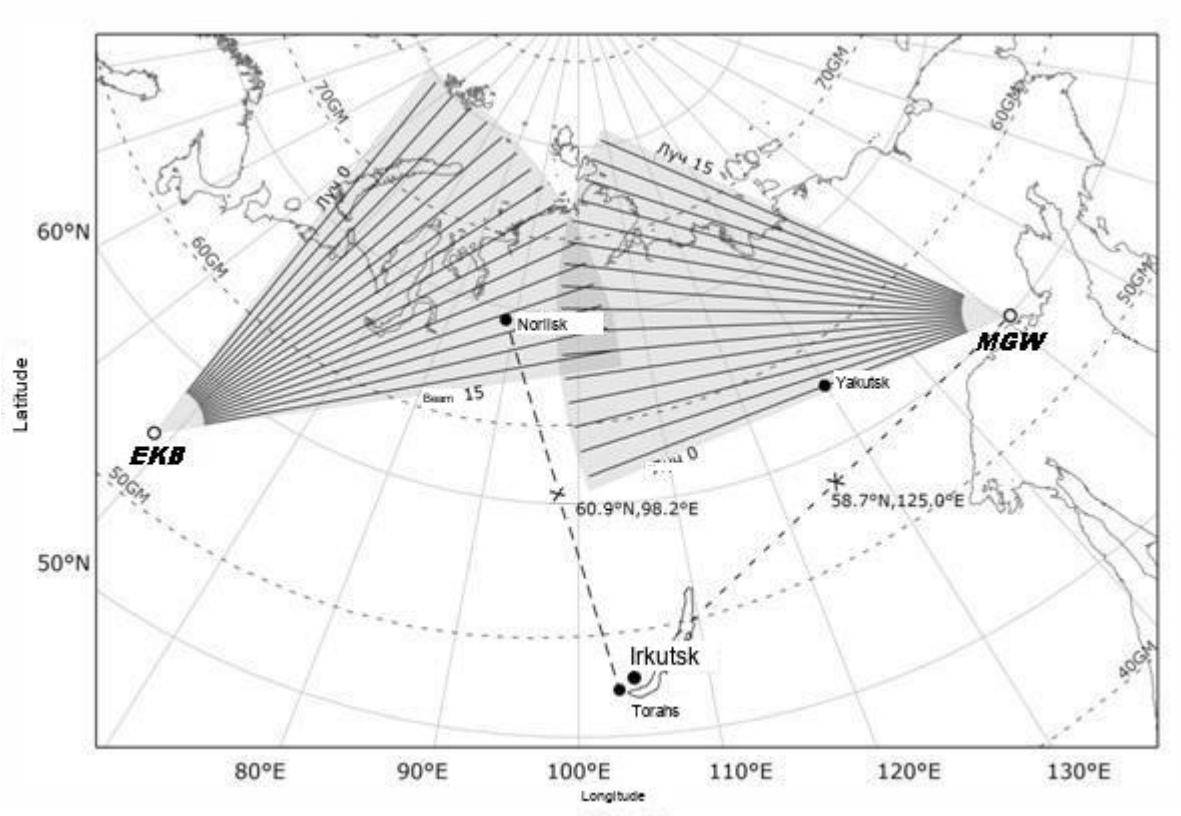
60°N
50°N
Latitude
80°E
90°E
100°E
110°E
120°E
130°E
Longitude
70GM
60GM
50GM
40GM
Луч 0
Луч 15
Beam 15
Norilsk
Yakutsk
Irkutsk
Torans
EKB
MGW
60.9°N,98.2°E
58.7°N,125.0°E

Fig. 2

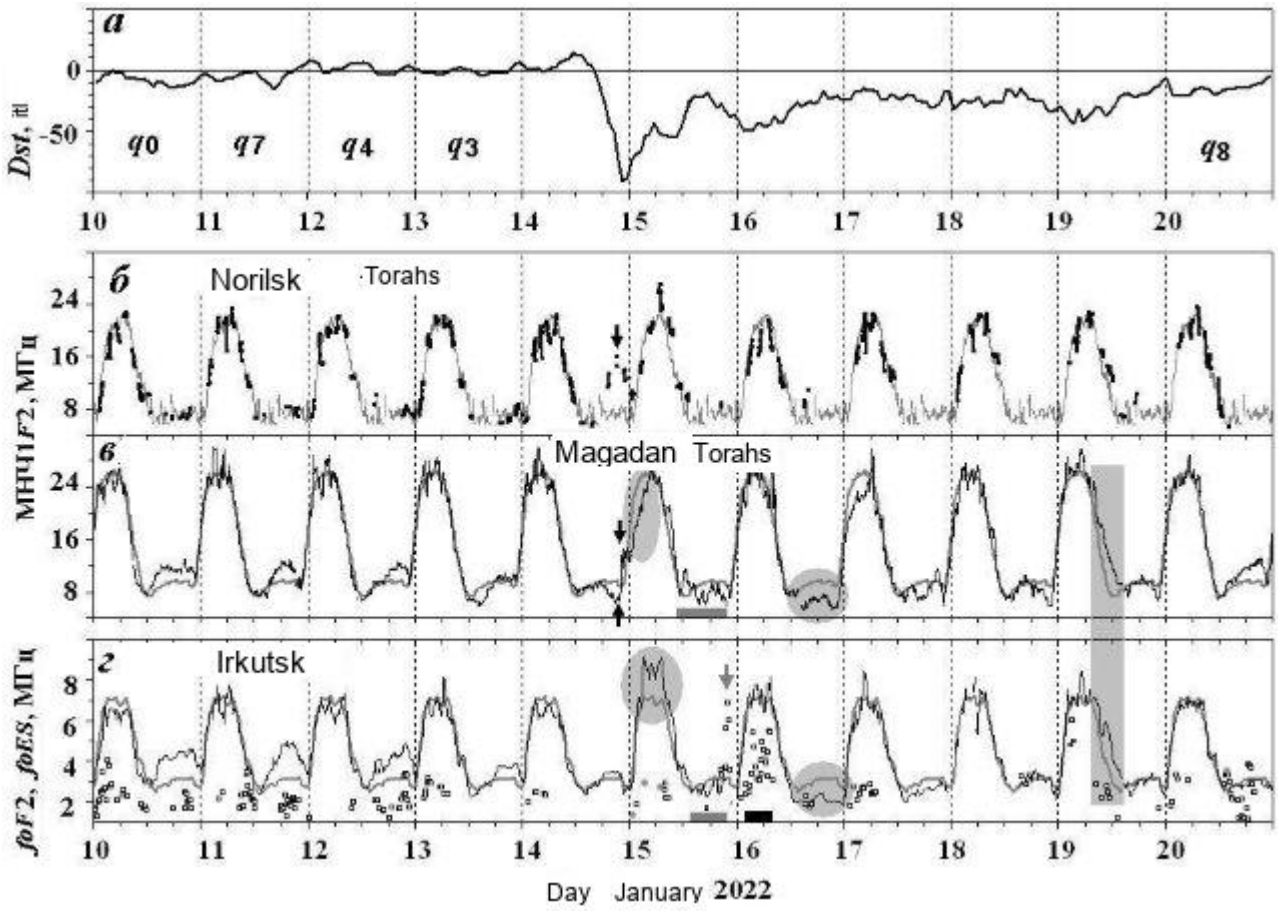
а
Dst, нТл
0
-50
q0
q7
q4
q3
q8
10
11
12
13
14
15
16
17
18
19
20
б
Norilsk
Torahs
в
Magadan
Torahs
МНЧ1F2, МГц
24
16
8
г
Irkutsk
foF2, foEs, МГц
8
6
4
2
Day January 2022

Fig. 3

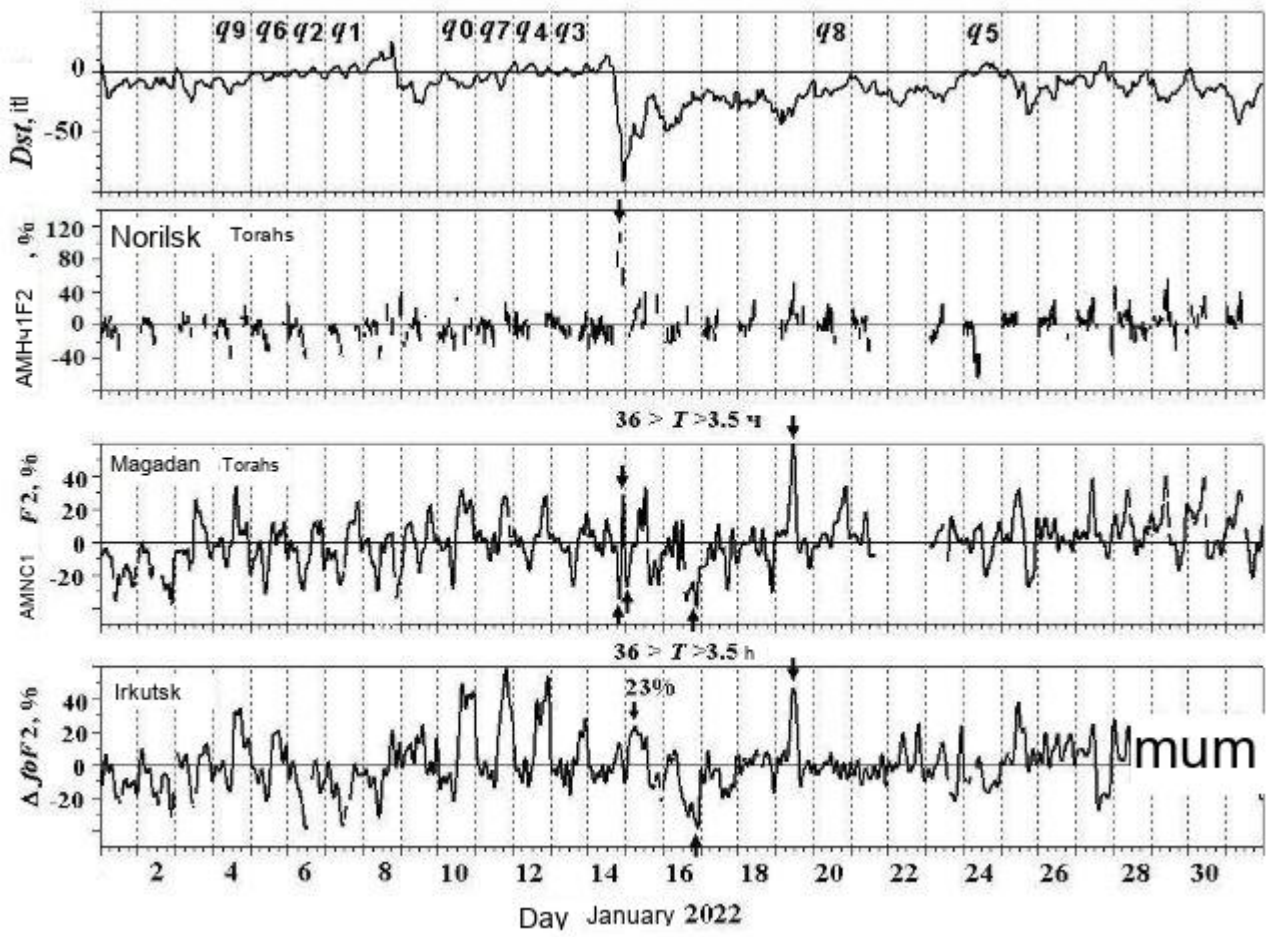
q9 q6 q2 q1
q0 q7 q4 q3
q8
q5
Dst, itl
0
-50
Norilsk
Torahs
AMHч1F2 , %
120
80
40
0
-40
36 > T >3.5 ч
Magadan
Torahs
AMNC1 F2, %
40
20
0
-20
36 > T >3.5 h
Irkutsk
23%
Δ foF2, %
mum
2
4
6
8
10
12
14
16
18
20
22
24
26
28
30
Day January 2022

Fig. 4

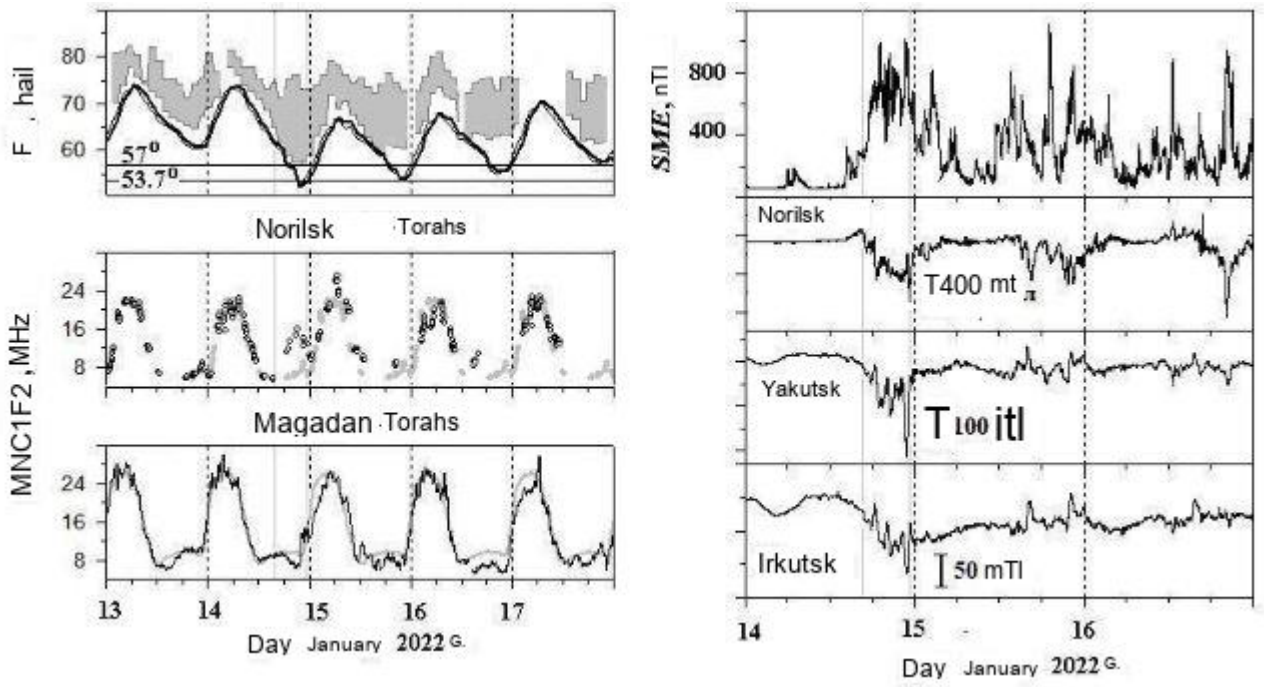
F , hail
80
70
60
57°
53.7°
Norilsk
Torahs
MNC1F2 , MHz
24
16
8
Magadan
Torahs
13
14
15
16
17
Day January 2022 G.
SME, nTl
800
400
Norilsk
T400 mt
Yakutsk
T100 itl
Irkutsk
50 mTl
14
15
16
Day January 2022 G.

Fig. 5

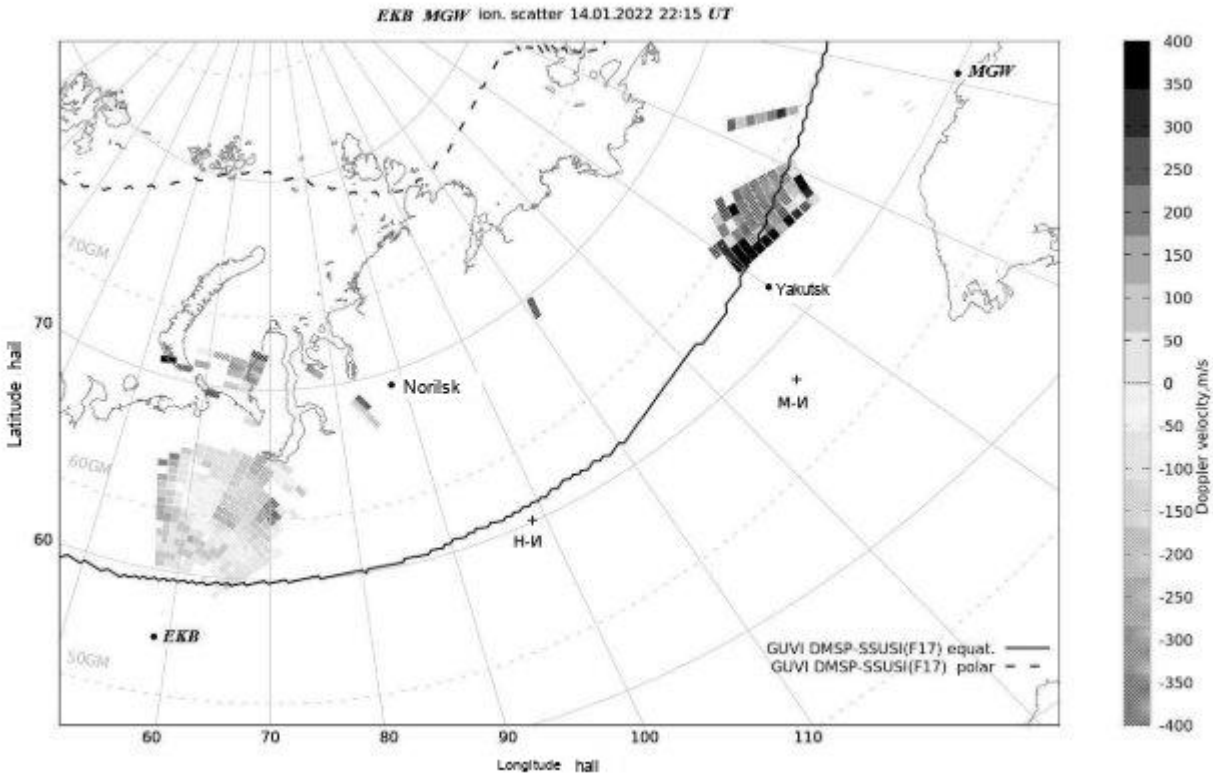
EKB MGW ion. scatter 14.01.2022 22:15 UT
MGW
Yakutsk
Norilsk
М-И
Н-И
EKB
70GM
60GM
50GM
GUVI DMSP-SSUSI(F17) equat.
GUVI DMSP-SSUSI(F17) polar
Latitude hall
Longitude hall
Doppler velocity,m/s
400
350
300
250
200
150
100
50
0
-50
-100
-150
-200
-250
-300
-350
-400
60
70
80
90
100
110

Fig. 6.

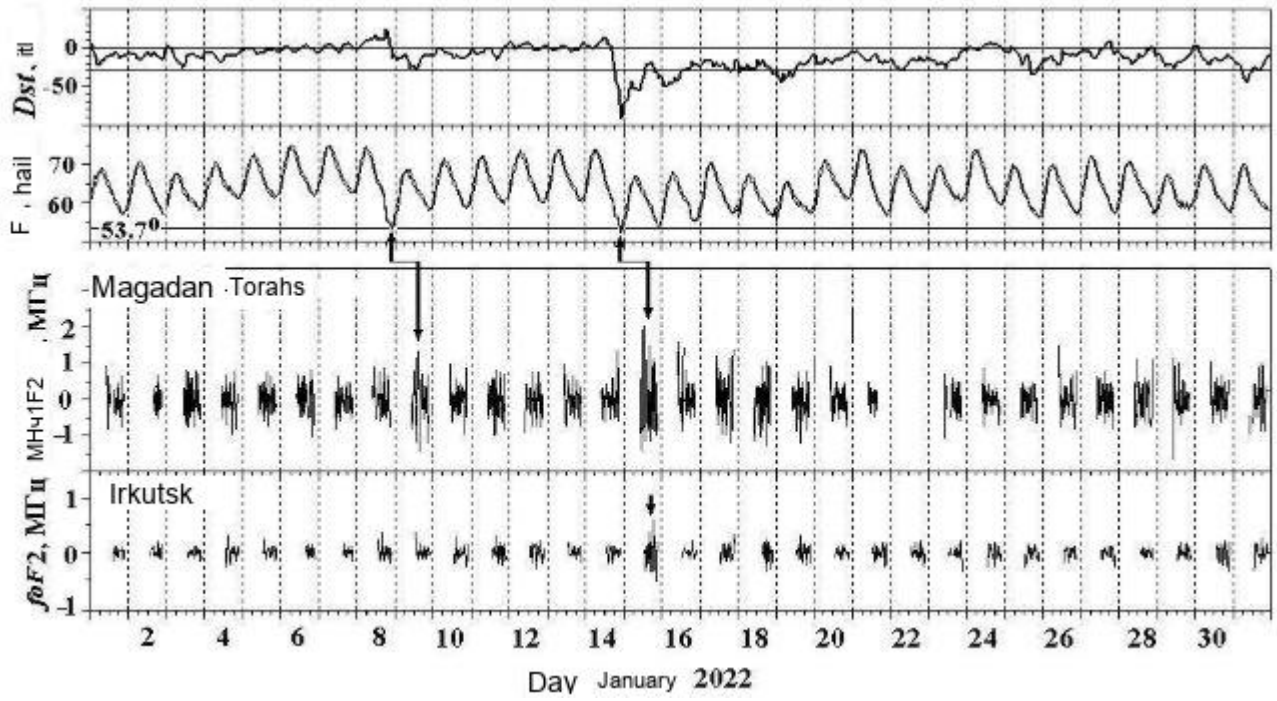
Dst, нТл
0
-50
F , hail
70
60
53,7°
Magadan
Torahs
МГц
2
1
0
-1
MHч1F2
Irkutsk
foF2, МГц
1
0
-1
2 4 6 8 10 12 14 16 18 20 22 24 26 28 30
Day January 2022

Fig. 7.

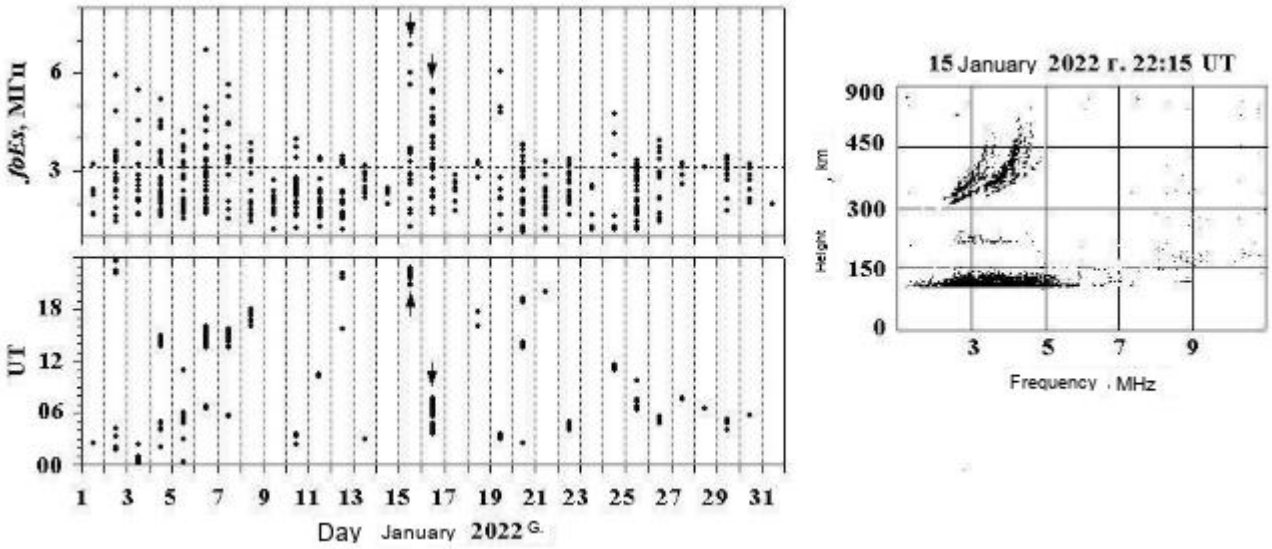
foEs, МГц
6
3
UT
18
12
06
00
1 3 5 7 9 11 13 15 17 19 21 23 25 27 29 31
Day January 2022 G.
15 January 2022 г. 22:15 UT
900
450
300
150
0
Height , km
3 5 7 9
Frequency , MHz

Fig. 8.

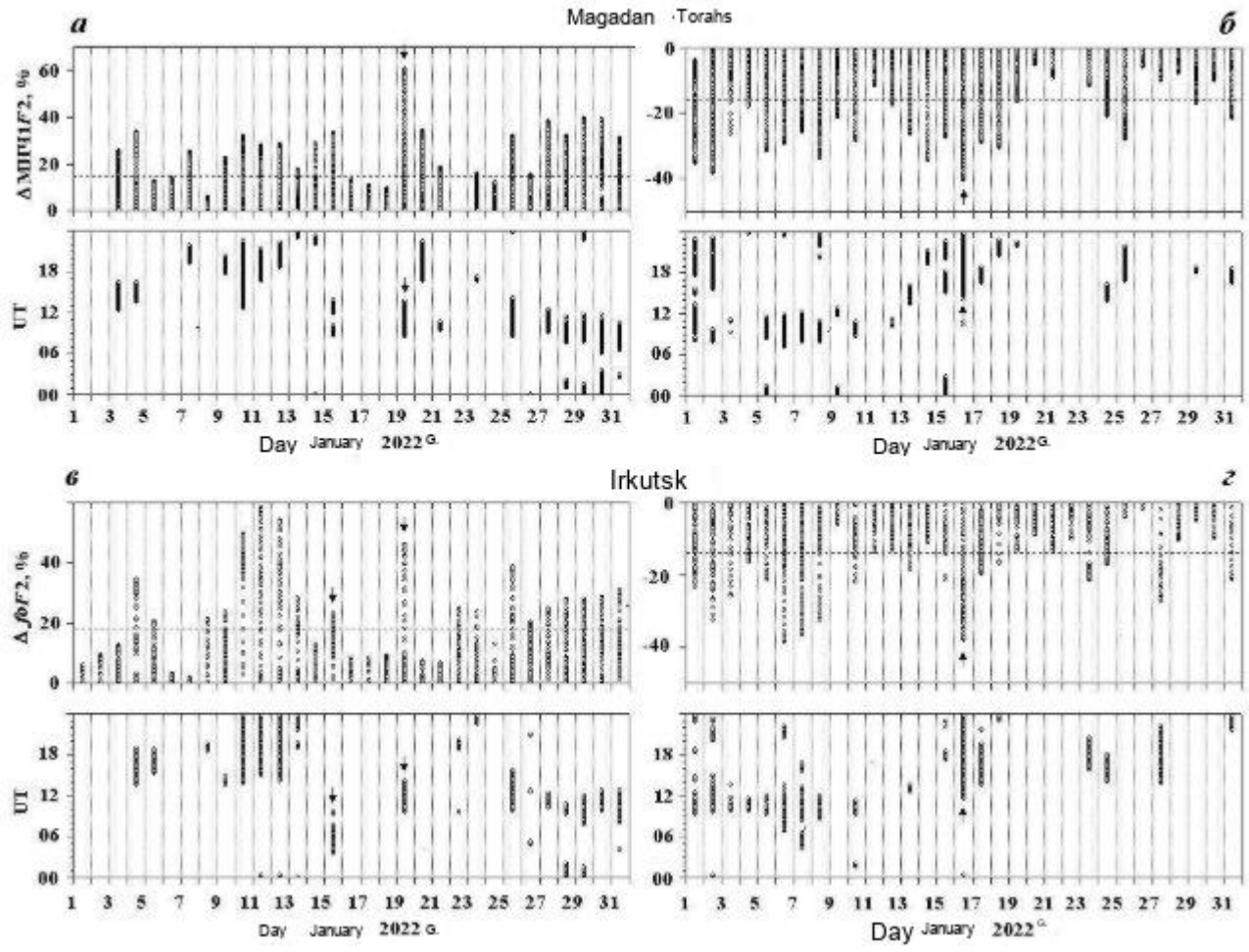
а
Magadan
Torahs
б
ΔMUF2, %
UT
Day January 2022 G.
в
Irkutsk
г
ΔfoF2, %

Fig. 9.

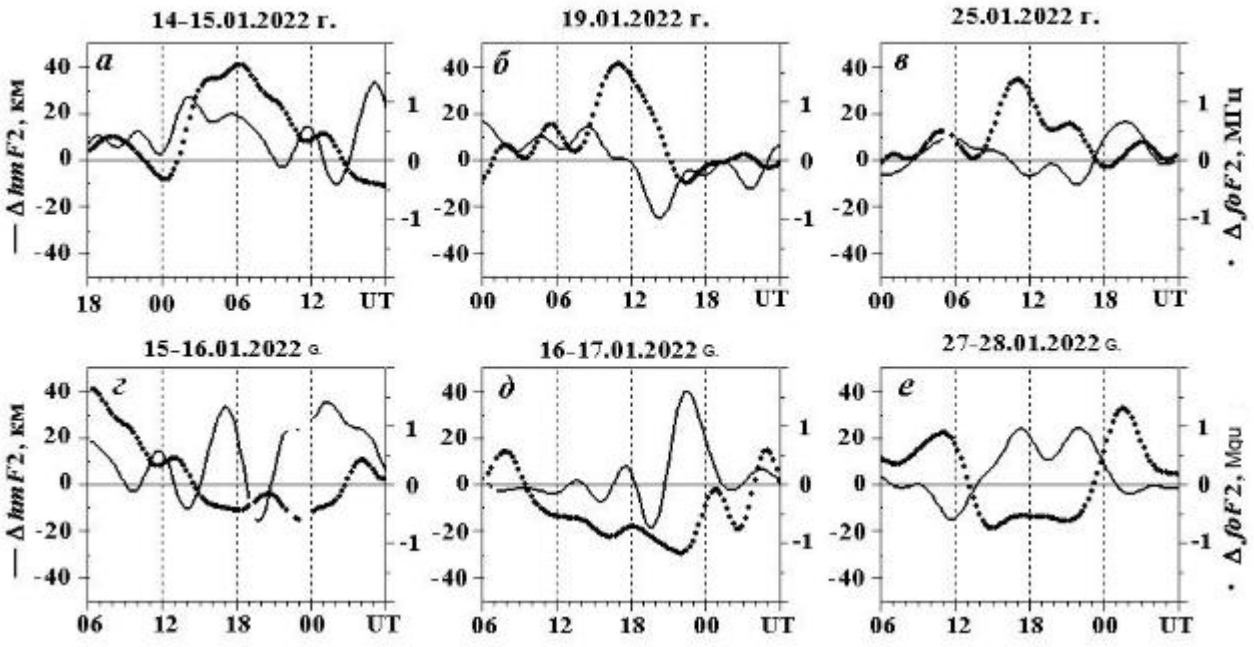
14–15.01.2022 г.
19.01.2022 г.
25.01.2022 г.
15–16.01.2022 г.
16–17.01.2022 г.
27–28.01.2022 г.
а
б
в
г
д
е
— Δ hmF2, км
· ΔfoF2, МГц
· ΔfoF2, Mgu
40
20
0
-20
-40
1
0
-1
18
00
06
12
UT

Fig. 10.